J Mater Sci (2018) 53:12741–12749

Ceramics

Influence of galia (Ga_2O_3) addition on the phase transformations and crystal growth behavior of zirconia (ZrO_2)

Chen Barad[1,2], Giora Kimmel[3], Hagay Hayun[4], Dror Shamir[5], Michael Shandalov[5], Gal Shekel[5], and Yaniv Gelbstein[1,4,*]

[1] *The Unit of of Energy Engineering, Ben-Gurion University of the Negev, 84105 Beer-Sheva, Israel*
[2] *Israel Atomic Energy Commission (IAEC), P.O. Box 7061, 61070 Tel Aviv, Israel*
[3] *Institutes for Applied Research, Ben-Gurion University of the Negev, 84105 Beer-Sheva, Israel*
[4] *Department of Materials Engineering, Ben-Gurion University of the Negev, 84105 Beer-Sheva, Israel*
[5] *NRCN, P.O. Box 9001, 84190 Beer-Sheva, Israel*

Received: 29 April 2018
Accepted: 7 June 2018
Published online: 11 June 2018

ABSTRACT

The effect of a galia (Ga_2O_3) addition on the crystallographic phase evolution and the crystal growth behavior of zirconia (ZrO_2) rich powder were investigated. Binary compositions of galia–zirconia powder (on the zirconia-rich side of the quasi-binary phase diagram) were obtained by the sol–gel method and calcined at different temperatures for 2 h. Rietveld refinement (FullProf program) was used to determine the crystallographic phase composition. Crystal size was approximated based on X-ray diffractions analysis combined with estimates of average crystal size obtained by processing high-resolution scanning electron microscopy images. The surface area of the powders obtained was measured via the Brunauer–Emmett–Teller method. Zirconia–galia sol–gel powders were found to form tetragonal or mixed tetragonal–monoclinic solid solution phases depending on both composition and calcination temperature. It was shown that galia suppressed crystal growth process in zirconia, producing finer nano-powders with higher surface area compared to pure zirconia.

Introduction

Pure zirconia follows a monoclinic ($P2_1/c$) → tetragonal ($P42/nmc$) → cubic ($Fm3m$) phase transition sequence upon heating [1]. The monoclinic phase transformation is avoided by stabilizing the tetragonal or cubic phase by doping with yttria (Y_2O_3) depending on its molar fraction. Zirconia-based materials are used widely in solid oxide fuel cells, medicine, catalysts, etc. [2–4]. From a mechanical point of view, the tetragonal phase has more practical applications than the cubic phase [5]. Pure galia (Ga_2O_3) has five polymorphs: α, β, γ, δ and ε, of which the β polymorph β-Ga_2O_3 (monoclinic galia) is

Address correspondence to E-mail: yanivge@bgu.ac.il

https://doi.org/10.1007/s10853-018-2556-1

stable in its entire temperature range up to the melting point [6]. While galia is a poor thermal and electrical conductor, in reducing conditions, it becomes an *n*-type semiconductor due to the formation of oxygen vacancies [6, 7].

Recent literature has repeatedly mentioned that investigations into the quasi-binary zirconia–galia system are gravely lacking and the works regarding this system are insufficient [8, 9]. The studies that do exist are not updated [10, 11]. The current research is inspired by landmark studies on the zirconia–alumina system where it has been reported that alumina has a tendency to suppress crystal growth in zirconia–alumina powder, allowing a preservation of crystal size in the lower nano-range as compared to non-doped zirconia, which exhibits more extensive crystal growth [12, 13]. The slow grain growth in doped zirconia is attributed to solute ion segregation into the grain boundaries inhibiting the grain growth. For instance, it was shown that faster powder sintering and reduced sintering temperature was required for densification of zirconia-doped alumina solutions [14]. Similar trends have been reported [15, 16] upon the addition of small amounts of galia to samaria-(Sm_2O_3) doped ceria (CeO_2) and to yttria-doped ceria. The preparation of ultra-fine powders with a smaller particle size is significant, among others, for decreasing sintering temperature and improving densification and mechanical properties. Gallium has similarities to aluminum and yet remains on the outskirts of the mixed oxides field, whereas zirconia–alumina system has been researched in depth [17–21]. In this study, the influence of galia addition to zirconia-rich powders was investigated regarding the crystallographic phase transformations and the connection between the concentration of galia and calcination temperature on the crystal size and surface area.

Materials and methods

Sample preparation

Powder batches were synthesized via the sol–gel method based on the one reported in Kuo et al. [22] using different precursor salts to form zirconia–galia powders: zirconium oxynitrate hydrate ($ZrO(NO_3)_2 \cdot 2H_2O$) (purity ~ 99%) and gallium nitrate octahydrate ($Ga(NO_3)_3 \cdot 8H_2O$). The sol–gel method is a robust and simple method allowing the preparation of zirconia powders with versatile contents of galia. The solution of the precursors was made by dissolving stoichiometric amounts of precursors in deionized water (18.3 MΩ cm resistance) at room temperature. Ammonium hydroxide solution (1.5 M) was dripped slowly into the mixture under continuous stirring. The dripping continued until the pH value was 9. The gel's precipitates were rinsed with deionized water. Eventually, the wet precipitates were dried using freeze-drying technique [23]. The gel was indirectly frozen by placing it in a closed beaker, which was submerged into liquid nitrogen and then freeze-dried at 223 K in a vacuum chamber. Each zirconia–galia powder was then divided into different samples which were calcined in air using alumina crucibles for 2 h at different temperatures. The different compositions obtained were ZrO_2 with: 0, 0.7, 2, 3, 5, 7, 14 and 100 mol% of Ga_2O_3.

Phase composition analysis was performed using X-ray diffraction (XRD). The crystal size of zirconia–galia powders was approximated using three different methods: Brunauer–Emmett–Teller (BET) analysis, for the lower nano-range, XRD analysis, using the Williamson–Hall approach, for the intermediate nano-range (below 60 nm) and high-resolution scanning electron microscopy (HR-SEM) using *ImageJ* (image processing software) in the higher nano-range (above 60 nm).

Sample characterization

The composition analysis of the sol–gel powder was investigated by inductively coupled plasma optic emission spectroscopy (ICP-OES; Spectro Arcos, Kleve, Germany). The crystalline phase composition was determined by X-ray diffraction analysis (XRD; DMAX 2100 powder diffractometer, Rigaku, Japan) upon applying the Rietveld refinement. The surface area of powder was measured by BET (Brunauer–Emmett–Teller) method (NOVAtouch^{TM}, surface area and pore size analyzer, TouchWin^{TM} software version 1.0, Quantachrome Instruments, USA). Sample preparation for BET analysis included outgassing of samples in vacuum under heating to a maximum temperature of 573 K and using nitrogen at 77 K for obtaining adsorption isotherms. The morphology of the powder after calcination was examined using a high-resolution scanning electron microscope (HR-SEM; JSM-7400, JEOL, Tokyo, Japan). Crystal size in

the higher nano-range (above 60 nm) was approximated based on the measurement of more than 150 well-defined crystals apparent in the HR-SEM images using *ImageJ* (image processing software, National Institutes of Health, Bethesda, MD, USA).

Results and discussion

ICP-OES results confirmed that following the sol–gel synthesis, the powder composition well agreed with the theoretical design. The results are shown in Table 1.

XRD analysis was the key tool for mapping the phase compositions as a function of the galia concentration and calcination temperature. The XRD patterns of zirconia with different molar concentrations of galia are shown in Fig. 1, and the representative Rietveld refinements are shown in Fig. 2.

Figure 3 shows a mapping of the different phase compositions obtained from the Rietveld analysis on a diagram of the calcination temperature as a function of the molar percentage of galia in the range of 0–14 mol%, where "m" refers to monoclinic phase and "t" to tetragonal phase. The mass fraction of each phase for multi-phases is shown in parentheses.

Investigation of the XRD patterns in Fig. 1 reveals that the addition of galia to zirconia resulted in a considerable peak broadening and had a major influence on the crystallization temperature. Such a broadening can be easily seen upon calcination at 673 K of 0.7 mol% galia (Fig. 1b) compared to pure zirconia (Fig. 1a) or upon calcination at 873 K of 5 mol% galia (Fig. 1e) compared to 3 mol% galia (Fig. 1d). It can be also seen that a quasi-amorphous structure is obtained after calcination at 673 K for 2 h when adding 0.7 mol% galia to zirconia. When adding 5 mol% galia to zirconia, the same structure is maintained after calcination at a higher temperature of 873 K.

For each given concentration of galia in zirconia, it can be observed that the calcination temperature influences the crystalline domain size as the diffraction peaks become sharper as temperature rises and larger crystals were grown. Figure 3 shows that the addition of galia to zirconia stabilizes completely or partially the tetragonal phase depending on its concentration and calcination temperature. This finding is in agreement with the inability of galia to stabilize the cubic polymorph in the zirconia–galia system as was also previously reported [9]. From Fig. 3, for 14 mol% galia calcined at temperatures of 1273 and 1473 K, a monoclinic gallium oxide phase (C2/m) was segregated. From analysis of Fig. 1h, the monoclinic crystallization of pure galia starts in the range of 873–923 K in accordance with previously reported data [24]. For calcination temperatures of 673 and 873 K, the cubic spinel-type γ-Ga_2O_3 was obtained, and for higher temperatures of 923, 1073, 1473 K, the stable monoclinic β-Ga_2O_3 polymorph was formed. The monoclinic structure was detected in the 0.7 and 2 mol% galia compositions calcined at 1073–1473 K and in the > 2 mol% galia compositions calcined at 1273–1473 K for 2 h. Therefore, as the concentration of galia increases, the appearance of the monocline phase is delayed and diminished. For lower calcination temperatures, the monoclinic phase appearance was avoided and a single tetragonal zirconia phase was detected (as shown in Fig. 3). Table 2 shows the tetragonal unit cell parameters and volume based on the Rietveld results.

Table 2 shows that for a given calcination temperature, the unit cell's volume decreased as the concentration of galia increased.

Regarding the powder morphology, when tetragonal crystals transformed into monoclinic, twins were started to form as demonstrated in Fig. 4. A closer investigation of this figure reveals that although some of the large crystalline domains were twinned, twinning was much more emphasized in the smaller

Table 1 ICP-OES results

Theoretical % mol of Ga_2O_3	ICP-OES result—% mol of Ga_2O_3
0.7	0.74
2	2.0
3	3.2
5	5.5
7	6.9
14	14.4

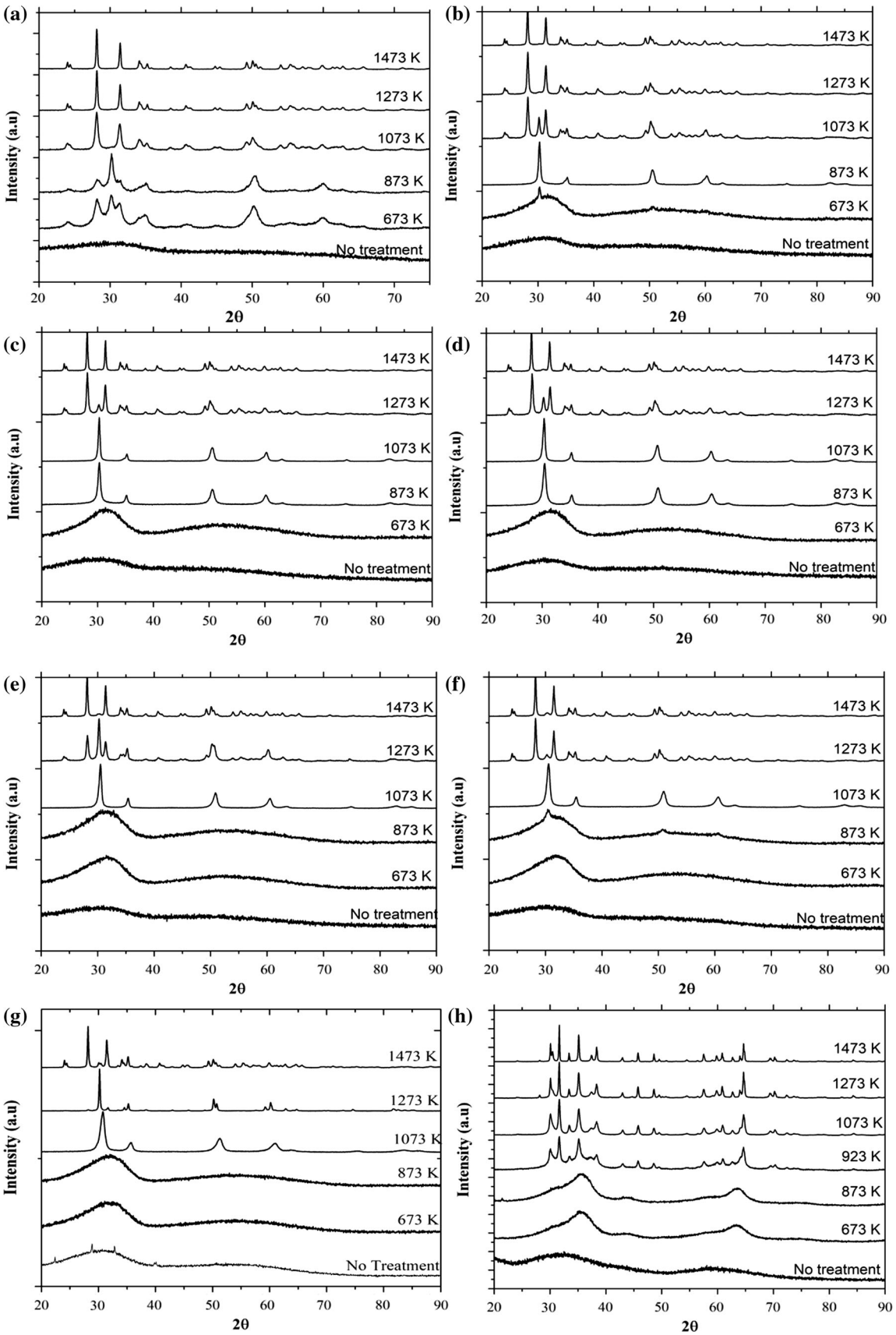
(a)
1473 K
1273 K
1073 K
873 K
673 K
No treatment
Intensity (a.u)
2θ
(b)
1473 K
1273 K
1073 K
873 K
673 K
No treatment
Intensity (a.u)
2θ
(c)
1473 K
1273 K
1073 K
873 K
673 K
No treatment
Intensity (a.u)
2θ
(d)
1473 K
1273 K
1073 K
873 K
673 K
No treatment
Intensity (a.u)
2θ
(e)
1473 K
1273 K
1073 K
873 K
673 K
No treatment
Intensity (a.u)
2θ
(f)
1473 K
1273 K
1073 K
873 K
673 K
No treatment
Intensity (a.u)
2θ
(g)
1473 K
1273 K
1073 K
873 K
673 K
No Treatment
Intensity (a.u)
2θ
(h)
1473 K
1273 K
1073 K
923 K
873 K
673 K
No treatment
Intensity (a.u)
2θ

◀**Figure 1** XRD patterns of: **a** pure ZrO_2, **b** ZrO_2 + 0.7 mol% Ga_2O_3, **c** ZrO_2 + 2 mol% Ga_2O_3, **d** ZrO_2 + 3 mol% Ga_2O_3, **e** ZrO_2 + 5 mol% Ga_2O_3, **f** ZrO_2 + 7 mol% Ga_2O_3, **g** ZrO_2 + 14 mol% Ga_2O_3 and **h** pure Ga_2O_3 at different calcination temperatures calcined for 2 h.

crystalline domains. The transformation from tetragonal phase into monoclinic phase is followed by formation of hydrostatic pressure and strains since monoclinic zirconia has lower density and thus requires more volume [1]. Large crystals apply pressure on smaller crystals which transform into the monoclinic phase due to mechanical deformation, while the large crystals transformed into the monoclinic phase in thermal transformation.

The crystallite size was calculated via the Williamson–Hall plot:

$$\beta \cdot \cos(\theta) = k \cdot \lambda / L + 4 \cdot \varepsilon \cdot \sin(\theta), \quad (1)$$

where β is the broadening of the diffraction line measured at half of the maximum intensity, λ is the wavelength (Cu-κα), θ is the Bragg angle for a given diffraction and k is a constant, which is in general equal to 0.94 for powders. The instrumental broadening effect was estimated by subtracting the full width at half maximum of a standard sample (LaB_6) from β of the respective Bragg peaks. L represents the crystallite size, and ε represents the lattice strain. The characteristic Williamson–Hall plot corresponds to the graph of $\beta \cdot \cos(\theta)$ versus $\sin(\theta)$. After data collection, a linear regression should give a linear fit. The

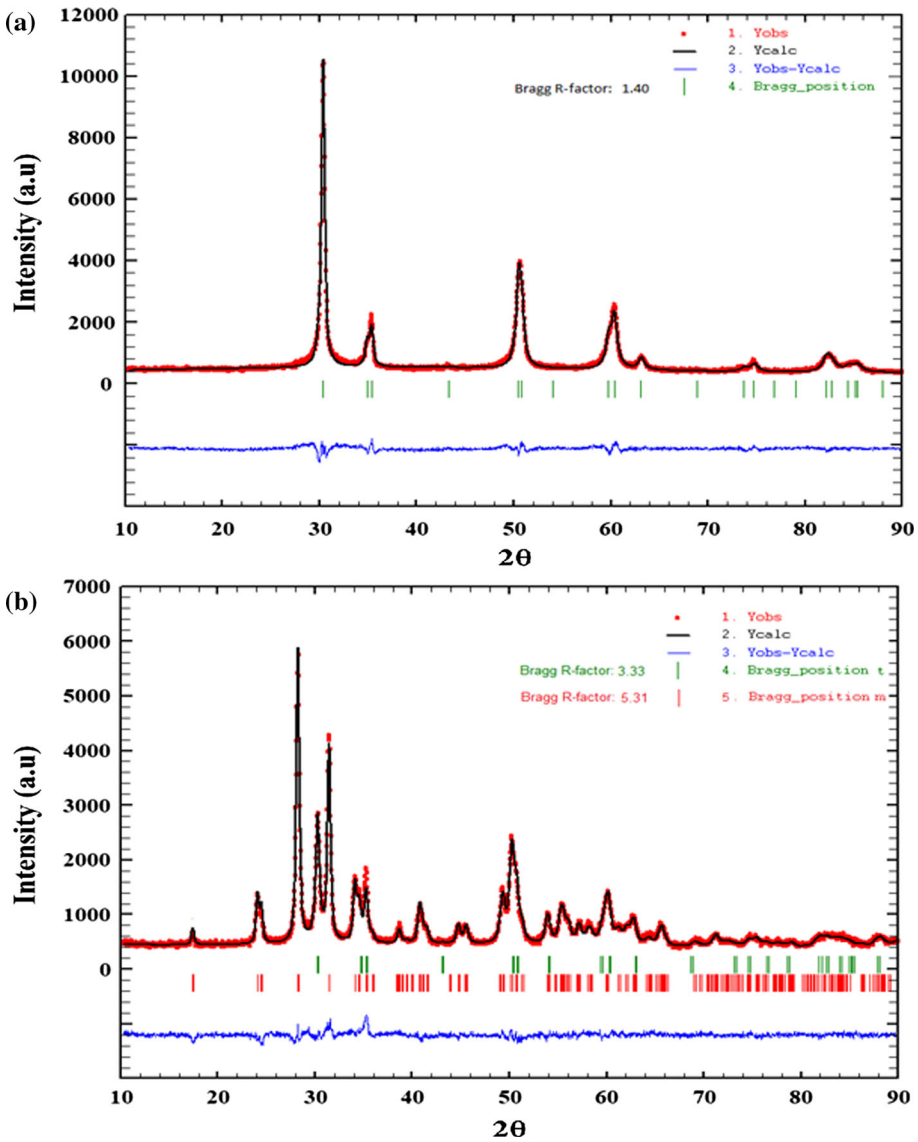

Figure 2 Rietveld refinements of **a** ZrO_2 + 0.7 mol% Ga_2O_3 calcined at 873 K and **b** ZrO_2 + 5 mol% Ga_2O_3 calcined at 1273 K for 2 h.

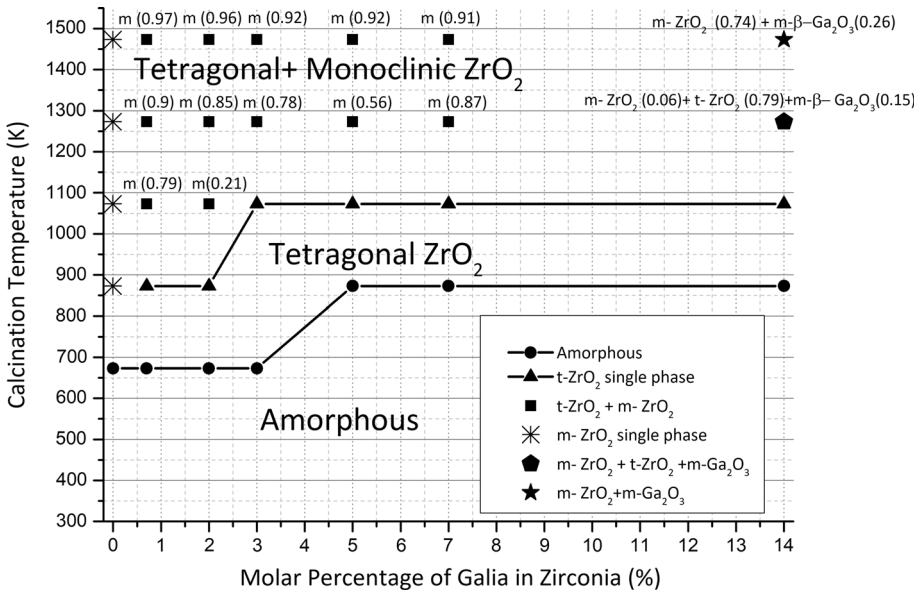

Figure 3 Rietveld analysis results of the crystallographic phases obtained after calcination at different temperatures for 2 h.

Table 2 Refined unit cell parameters values of the t-ZrO_2 solid solutions

% mol of Ga_2O_3	Calcination temperature (K)	a (Å)	c (Å)	Cell volume (Å^3)
0.7	873	3.591	5.140	66.271
2	873	3.608	5.082	66.155
3	873	3.591	5.099	65.749
	1073	3.592	5.119	66.027
5	1073	3.595	5.078	65.632
7	1073	3.592	5.055	65.211
14	1073	3.578	5.058	64.753

crystallite size was extracted from the y-intercept of the $(k \cdot \lambda/L)$ fit. The Williamson–Hall approach becomes less accurate when crystals are bigger than approximately 60 nm and therefore, HR-SEM images were analyzed based on measuring the crystal size distribution. The average crystal size obtained for zirconia with 14 mol% galia calcined at 1073 K for 2 h (as a representative case) was estimated as 20 nm and was also cross-checked by HR-SEM which provided a similar average value.

Following the same calcination temperature of 1073 K, the 0.7% mol galia composition exhibited larger crystals in the size range of 40–55 nm (as derived from XRD crystal size analysis and HR-SEM image processing), highlighting the effect of galia on inhibiting crystalline domains growth. Investigating the average crystal size at the highest calcination temperature tested of 1473 K as was measured from the HR-SEM images using ImageJ image software clearly indicated a reduction trend from approximately 400 nm for 0.7 mol% galia, to 300 and 200 nm for powders containing 7 and 14 mol% galia, respectively, highlighting again the domains growth effect of galia (Fig. 5).

BET (Brunauer–Emmett–Teller) measurements were carried out to pre-calcined galia-doped powders in order to confirm the effects found by XRD. Powders showed surface area in the range of 110–150 m^2/g. Figure 6 shows that surface area increased with increase of the concentration of galia. The increase in surface area is an indication to the decrease in powder particle size.

Following 1473 K calcination, nano-agglomerated particles with irregular shapes were observed by HR-SEM, as can be seen in Fig. 7a for the secondary electron (SE) and Fig. 7b the backscattered electrons (BSE) investigation modes of the 14 mol% galia composition. Energy-dispersive X-ray spectroscopy (EDS) of these micrographs indicated the presence of monoclinic zirconia (brighter phase in Fig. 7b) and monoclinic galia (darker phase in Fig. 7b), in

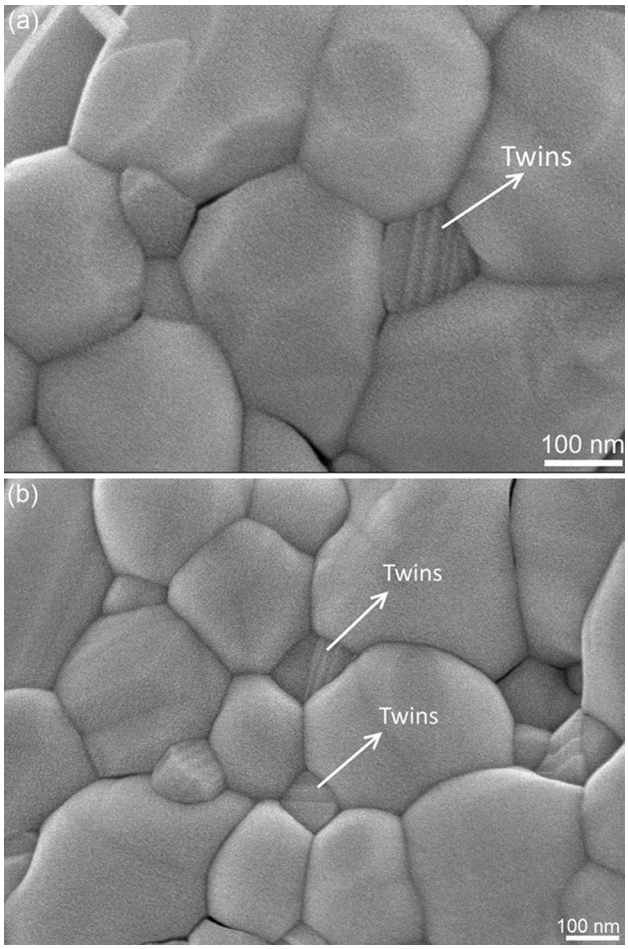

Figure 4 HR-SEM of powders calcined at 1473 K for 2 h: **a** ZrO_2 + 5 mol% and **b** ZrO_2 + 7 mol% Ga_2O_3.

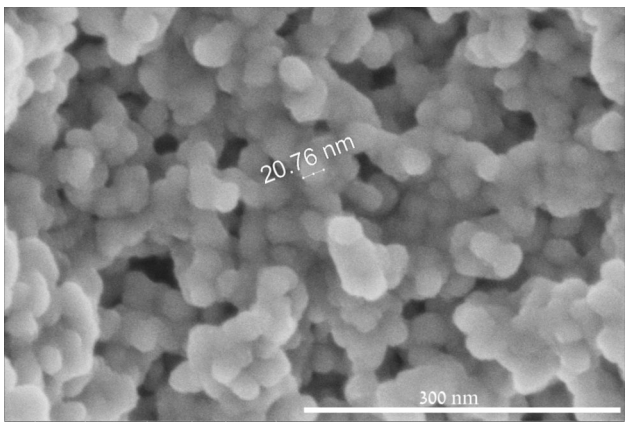

Figure 5 HR-SEM of zirconia with 14 mol% galia calcined at 1073 K for 2 h.

agreement with the XRD results in Fig. 3, indicating some precipitation of monoclinic galia.

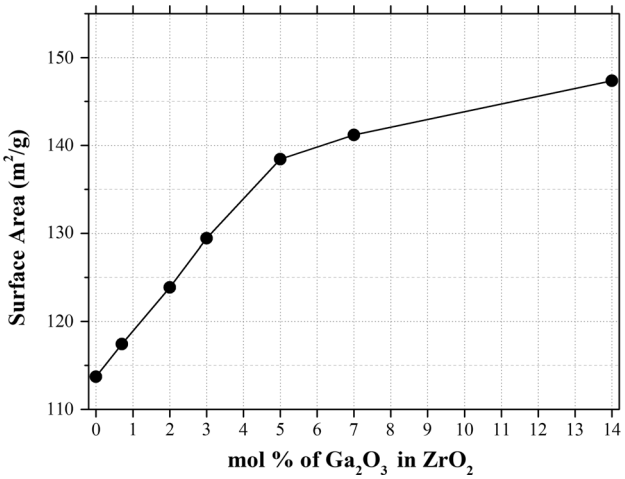

Figure 6 BET analysis for different contents of galia in zirconia.

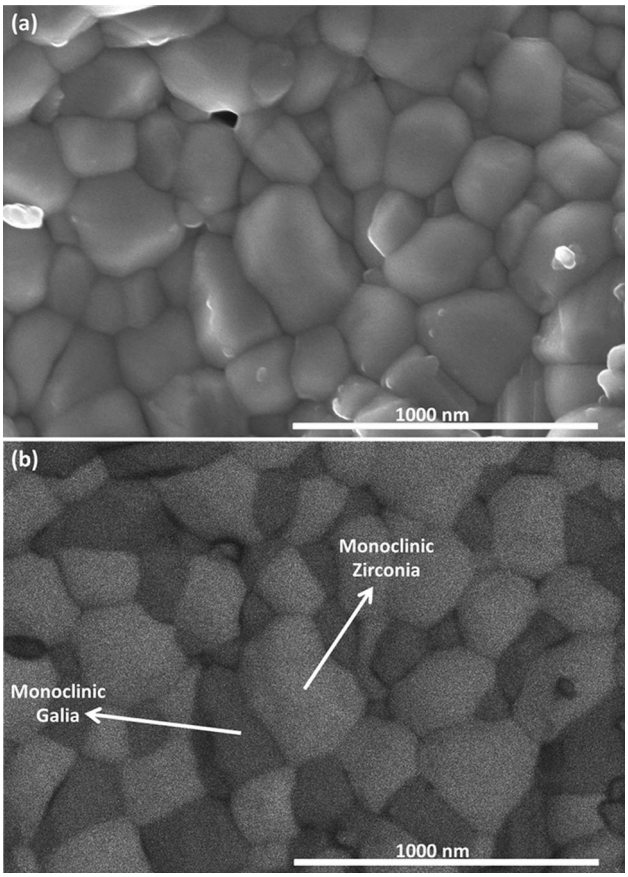

Figure 7 HR-SEM images of ZrO_2 + 14 mol% Ga_2O_3 calcined at 1473 K for 2 h: **a** SE image and **b** BSE image.

Conclusions

In the current research, zirconia–galia nano-powders were synthesized via the sol–gel method. Zirconia–galia-based compositions with galia content in range

of 0.7–7 mol% were found to form tetragonal (P42/*nmc*) or mixed tetragonal (P42/*nmc*)–monoclinic ($P2_1/c$) solid solution phases depending on the composition and calcination temperature. The addition of galia suppressed the crystallization of zirconia resulting in an extended amorphous range. Galia also decreased the crystalline domains size and correspondingly the powder particle size as the content of galia increased up to 14 mol%, resulting in finer nano-powders with higher surface area, compared to those previously reported for non-doped zirconia.

Acknowledgements

The authors thank the Ilse Katz Institute for Nanoscale Science and Technology in Ben Gurion University of the Negev for their technical help and services. The authors would like to thank Prof. N. Frage and Dr. M. Sokol for their technical cooperation with the freeze-drying system. The authors would like to thank Mr. Y. George and Dr. M. Harush for their technical help and consultation.

Compliance with ethical standards

Conflict of interest The work was supported by the Israel Ministry of Natural Infrastructures Energy and Water Resources Grant (3/15), No. 215-11-022.

References

[1] Garvie R, Hannink R, Pascoe R (1975) Ceramic steel? Nature 258:703–704

[2] Stambouli AB, Traversa E (2002) Solid oxide fuel cells (SOFCs): a review of an environmentally clean and efficient source of energy. Renew Sustain Energy Rev 6:433–455

[3] Manicone PF, Iommetti PR, Raffaelli L (2007) An overview of zirconia ceramics: basic properties and clinical applications. J Dent 35:819–826

[4] Yamaguchi T (1994) Application of ZrO_2 as a catalyst and a catalyst support. Catal Today 20:199–217

[5] Viazzi C, Bonino J, Ansart F et al (2008) Structural study of metastable tetragonal YSZ powders produced via a sol–gel route. J Alloys Compd 452:377–383

[6] Stepanov S, Nikolaev V, Bougrov V et al (2016) Gallium oxide: properties and applica a review. Rev Adv Mater Sci 44:63–86

[7] Binet L, Gourier D (1998) Origin of the blue luminescence of β-Ga_2O_3. J Phys Chem Solids 59:1241–1249

[8] Pushkar YN, Parenago O, Fionov A et al (1999) Paramagnetic complexes of the probe molecules with electron accepting sites on the surface of M2O3–ZrO 2:(M = Al, Ga). Colloids Surf Physicochem Eng Asp 158:179–187

[9] Štefanić G, Musić S (2008) Thermal behavior of the amorphous precursors of the ZrO_2–GaO 1.5 system. J Alloys Compd 460:444–452

[10] Barret P, Berthet P (1997) EXAFS study of nanocrystalline solid solutions synthesized in the ZrO_2–Ga_2O_3, System. J Phys IV 7:483–490

[11] Barret P, Berthet P (1997) Preparation and characterization of nanocrystalline ZrO_2–Ga_2O_3 solid solutions. J Phys III 7:C2-1141–C2-1142

[12] Kimmel G, Zabicky J, Goncharov E et al (2004) Phase mapping of multi-component oxides derived from sol–gel precursors. J Metastab Nanocryst Mater 20:576–581

[13] Kimmel G, Zabicky J (2008) Stability, instability, metastability and grain size in nanocrystalline ceramic oxide systems. Solid State Phenom 140:29–36

[14] Tekeli S, Erdogan M, Aktas B (2004) Influence of α-Al_2O_3 addition on sintering and grain growth behaviour of 8 mol% Y_2O_3-stabilised cubic zirconia (c-ZrO_2). Ceram Int 30:2203–2209

[15] Yoshida H, Miura K, Fujita J et al (1999) Effect of gallia addition on the sintering behavior of samaria-doped ceria. J Am Ceram Soc 82:219–221

[16] Seo S, Park J, Park M et al (2014) Effects of gallia addition on sintering behavior and electrical conductivity of yttria-doped ceria. Electron Mater Lett 10:791–794

[17] Alexander KB, Becher PF, Waters SB et al (1994) Grain growth kinetics in alumina–zirconia (CeZTA) composites. J Am Ceram Soc 77:939–946

[18] De Aza A, Chevalier J, Fantozzi G et al (2002) Crack growth resistance of alumina, zirconia and zirconia toughened alumina ceramics for joint prostheses. Biomaterials 23:937–945

[19] Jayaseelan DD, Rani DA, Nishikawa T et al (2000) Powder characteristics, sintering behavior and microstructure of sol–gel derived ZTA composites. J Eur Ceram Soc 20:267–275

[20] Sarkar D, Mohapatra D, Ray S et al (2007) Synthesis and characterization of sol–gel derived ZrO_2 doped Al_2O_3 nanopowder. Ceram Int 33:255–261

[21] Haneda M, Kintaichi Y, Shimada H et al (1998) Ga_2O_3/Al_2O_3 prepared by sol-gel method as a highly active metal oxide-based catalyst for NO reduction by propene in the presence of oxygen, H_2O and SO_2. Chem Lett 27

[22] Kuo C, Lee Y, Hung I et al (2008) Crystallization kinetics and growth mechanism of 8 mol% yttria-stabilized zirconia (8YSZ) nano-powders prepared by a sol–gel process. J Alloys Compd 453:470–475

[23] Barad C, Shekel G, Shandalov M et al (2017) Internal nano voids in yttria-stabilised zirconia (YSZ) powder. Materials 10:1440. https://doi.org/10.3390/ma10121440

[24] Taş AC, Majewski PJ, Aldinger F (2002) Synthesis of gallium oxide hydroxide crystals in aqueous solutions with or without urea and their calcination behavior. J Am Ceram Soc 85:1421–1429